Jurnal
Teknologi

Full Paper

TUBULAR LINEAR SWITCHED RELUCTANCE ACTUATOR: DESIGN AND CHARACTERIZATION

Mariam Md Ghazaly[a*], Yeo Chin Kiat[a], Chong Shin Horng[a], Norhaslinda Hasim[a], Zulkeflee Abdullah[b], Nurdiana Nordin[a]

[a]Fakulti Kejuruteraan Elektrik, Universiti Teknikal Malaysia Melaka, Hang Tuah Jaya, 76100 Durian Tunggal, Melaka, Malaysia
[b]Fakulti Kejuruteraan Pembuatan, Universiti Teknikal Malaysia Melaka, Hang Tuah Jaya, 76100 Durian Tunggal, Melaka, Malaysia

Article history
Received
29 October 2021
Received in revised form
15 June 2022
Accepted
15 June 2022
Published Online
21 August 2022

*Corresponding author
mariam@utem.edu.my

Graphical abstract

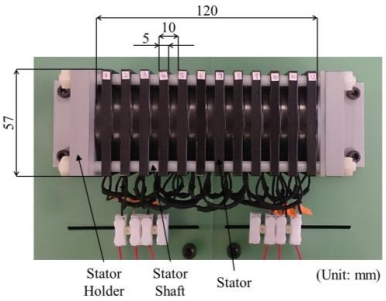

Abstract

Linear electromagnetic actuator is receiving significant attention due to recent advances in power electronics and modern control methods. This research proposes a three-phase tubular linear switched reluctance actuator (LSRA) for application in the semiconductor fabrication industry. The tubular LSRA has a robust construction, low manufacturing and maintenance cost, good fault tolerance capability, and high reliability in a harsh environment, making it an attractive alternative to a permanent magnet linear actuator. However, the tubular LSRA has a long mover, which increases the possibility of the mover deforming during fabrication. So, a new mover design is proposed to overcome the problem. The proposed mover design allows the traveling distance of the actuator to be modified by adding or removing the rings without changing the shaft. The tubular LSRA prototype is fabricated according to the optimized design. To drive the tubular LSRA, a appropriate switching algorithm method are used to provide the correct switching signal. This method is straightforward, while no extensive knowledge of power electronic converter is required. The developed tubular LSRA can generate a maximum static force of 0.65 N. Through the open-loop reciprocating motion, the dynamic responses of the tubular LSRA can achieve a maximum velocity of 210 mm/s and maximum acceleration of 8m/s^2, which are in the performance range for precision mechanism.

Keywords: Linear stage, tubular linear electromagnetic actuator, actuator design

Abstrak

Penggerak elektromagnet linear mendapat perhatian yang signikan disebabkan oleh kemajuan terkini dalam elektronik kuasa dan kaedah kawalan moden. Penyelidikan ini mencadangkan penggerak keengganan pensuisan linear tiga fasa berbentuk tiub (LSRA) untuk aplikasi dalam industri fabrikasi semikonduktor. LSRA berbentuk tiub ini mempunyai pembinaan yang teguh, kos pembuatan dan penyelenggaraan yang rendah, keupayaan toleransi kesalahan yang baik, dan kebolehpercayaan yang tinggi dalam persekitaran yang kasar, menjadikannya alternatif yang menarik kepada penggerak linear magnet kekal. Walau bagaimanapun, LSRA berbentuk tiub mempunyai reka bentuk penggerak yang panjang, di mana ini meningkatkan kemungkinan penggerak berubah bentuk semasa proses fabrikasi. Jadi, reka bentuk penggerak baharu dicadangkan untuk mengatasi masalah tersebut. Reka bentuk penggerak yang dicadangkan membolehkan jarak pergerakan penggerak diubah suai dengan menambah atau mengeluarkan gelang tanpa menukar aci. Dalam penyelidikan ini, prototaip LSRA berbentuk tiub direka mengikut reka bentuk yang dioptimumkan. Untuk memacu LSRA berbentuk tiub, kaedah algoritma pensuisan yang sesuai digunakan untuk memberikan isyarat pensuisan yang betul. Kaedah ini adalah mudah dan tidak memerlukan pengetahuan luas tentang penukar elektronik kuasa. LSRA berbentuk

tiub yang dibangunkan boleh menghasilkan daya statik maksimum 0.65 N. Melalui gerakan salingan gelung terbuka, tindak balas dinamik LSRA berbentuk tiub boleh mencapai halaju maksimum 210 mm/s dan pecutan maksimum 8m/s2, yang berada dalam julat prestasi untuk mekanisme ketepatan.

Kata kunci: Platform linear, penggerak elektromagnet tiub linear, reka bentuk penggera

1.0 INTRODUCTION

Linear synchronous actuator (LSA) has penetrated the market and established practical applications since hard and soft ferromagnetic material developments. The LSA structure consists of a stator with phase windings powered by the multiphase alternating current (AC) supply similar to a linear induction actuator, while permanent magnet and mover winding with direct-current (DC) supply are located on the mover for constant magnetic flux production to create the electromagnetic poles [1, 2]. The permanent magnet's presence caused the LSA to have a sizeable cogging force and normal force in planar LSA [3]. Moreover, high-energy rare-earth magnet progress can be up to 1.2T at room temperature and maximum operating temperature at 150 ˚C before the permanent magnet loses its magnetic properties [4-8]. However, the permanent magnet offers improved performance, especially in force density and dynamic response [9- 10].

A linear switched reluctance actuator (LSRA) is an electromagnetic actuator that operates based on the principle that magnetically salient poles on the mover are free to move to a position of minimum reluctance so that the flow of the magnetic flux can complete a magnetic circuit [11 - 13]. The LSRA possesses a simple structure in which the coil windings are located on the stator only, whilst the mover is made of ferromagnetic material without any coil winding or permanent magnet [14, 15]. The stator windings are fed regularly with a multiphase sequential DC supply for electromagnetic force production [16]. Besides that, the coil windings are concentrated rather than distributed. This setup will enable the LSRA to operate even if the phase winding is short-circuited. Since LSRA does not use the permanent magnet, the actuator has a low manufacturing cost and does not suffer from thermal drawbacks [17]. However, the high force ripple and high acoustic noise in the system deteriorates the performance, which restricts its application to precision devices [18-20].

Recent research has focused on developing the direct-drive linear switched reluctance actuator (LSRA) due to the increasing demand for low-cost, high-precision actuators from the manufacturing and semiconductor industries. This is because the permanent magnet has widely applied in the electromagnetic actuator, increasing the actuator's overall cost and difficulty in assembling the permanent magnet on the actuator due to the strong magnetic force. Besides that, the sizeable cogging force caused by the permanent magnet significantly deteriorates and affects the positioning and tracking accuracy of the precision actuator. LSRA eliminates the permanent magnet in the actuator structure, offering a simple geometrical structure that is easy to assemble and has no cogging force. However, this reduces the force density and efficiency of the LSRA.

On the other hand, most developed LSRAs focus on planar single-sided and planar double-sided structures. Planar single-sided LSRA exhibits significant normal force, resulting in high friction force and positioning error. Meanwhile, planar double-sided LSRA eliminates the normal force, but the force density is approximately 60% lower than the permanent magnet linear actuator, which limits the applications of LSRA. In contrast, the tubular LSRA can eliminate the normal force and enhance the force density compared to the planar type LSRA [21, 22]. However, a lack of attention has been paid to tubular LSRA, which causes the behaviour of the tubular LSRA, such as force and motion characteristics, to be unclear. Moreover, the conventional long mover increases the possibility of deforming during fabrication, affecting the tubular LSRA's performance. Therefore, an alternative design for the mover structure is required, while the characterization of the actuator is essential to understand the behaviour of the developed tubular LSRA.

2.0 METHODOLOGY

Design Optimization Procedure of Tubular LSRA

In this research, the actuator's parameters must be optimized to design the tubular LSRA with optimum performance. The optimization of the tubular LSRA has been carried out through the Finite Element Method (FEM) analysis by using Ansys Maxwell 3D version 18.0 software. The FEM analysis considers the nonlinearities such as material saturation, magnetic flux leakage, distribution, fringing effects, generated thrust force, and the complex geometry of the actuator with very accurate results. Therefore, this software is chosen to be used in this research to optimize the actuator's parameters based on the generated thrust force and

saturation effect. The optimization process will be carried out by applying the DC excitation current between 0 A to 2 A with an interval of 0.5 A. The output of the three phases is assumed to be similar during the optimization process. Hence, in this research only the single-phase excitation is applied to the tubular LSRA in the FEM analysis which is Phase A, whilst Phase B and Phase C were set at 0 A. By referring to the principles of electromechanical energy conversion, the generated thrust force, F in a magnetic circuit can be defined as in Equation 1.

$$F_y = \frac{1}{2} i^2 \frac{dL}{dy} \tag{1}$$

where F_y is generated thrust force, i is excitation current, L is phase inductance and mover position, y. Then, the phase inductance can be further derived as in Equation 2

$$L = \frac{\mu_o n^2 A}{g} \tag{2}$$

where μ_o is permeability of air, n is number of winding turns, A is overlapping area of magnetic flux path, g is air gap thickness. Furthermore, Ampere's circuit law defined the magnetomotive force (mmf), F, of an electromagnetic actuator which is related to the magnetic field is shown in Equation 3 to Equation 5.

$$F = \Phi \times R = n \times i \tag{3}$$

$$R_g = \frac{g}{\mu_o A_g} \tag{4}$$

$$R_i = \frac{l_i}{\mu_o \mu_i A_i} \tag{5}$$

where F is magnetomotive force, Φ is magnetic flux, R is magnetic reluctance, μ_i is permeability of material, l_i is material length, A_g is overlapping area of air gap and overlapping area of material, A_i. Based on Equation 1 to Equation 5, the number of winding turns and air gap thickness need to be optimized in this research. However, the number of winding turns will determine the magnetic co-energy, which affects the magnetic force and saturation level. Therefore, the number of winding turns is first optimized, followed by the air gap thickness. The output thrust force will be influenced by the overlapping area changes for both air gap and material. In order to achieve high generated force, the air gap thickness should be designed as small as possible, but the mechanical capability limits the slightest air gap. Other than that, it can be observed that the cross-sectional area is related to the number of pole pairs, tooth width, and mover tooth height of the designed tubular LSRA, which will affect the performance of the actuator.

The six parameters that will influence the output performance of the tubular LSRA will be discussed in the following sequence: (i) number of stator-to-mover pole pairs, (ii) number of winding turns, (iii) air gap thickness, (iv) mover tooth height, (v) pole width and (vi) types of material. The FEM analysis is conducted by manipulating these parameters one at a time while other parameters are fixed (remained). Figure 1 shows the optimization flowchart in which the sequential optimization method is adopted. The highest generated thrust force determines the optimized parameters of the tubular LSRA with the lowest magnetic flux saturation. The magnetic flux saturation can be observed by observing the saturation level of the generated thrust force. Therefore, the optimized parameters for tubular LSRA can be obtained and used for prototype fabrication based on the parameters as shown in Figure 2. The optimized parameters of the proposed tubular LSRA are summarized in Table 1. The tubular LSRA prototype was fabricated based on the optimized parameters so that the tubular LSRA has the optimum performance.

Tubular LSRA Prototype

In this research, a prototype of the proposed tubular LSRA was fabricated based on the FEM analysis results to verify the optimized design and evaluate the actuator performances. The tubular LSRA stator and mover fabrication were machined with a CNC lathe machine with a fabrication tolerance of 20 μm and were made of medium carbon steel, S45C. The fabricated stator is shown in Figure 3. The outer diameter (O.D) and the fabricated stator's inner diameter (I.D.) are 57 mm and 37 mm. The coil winding will be placed on the stator slot with a diameter and width of 37 mm and 2.5 mm. Then, twelve stators are mounted onto two stator holders attached to the main base. The stator's weight, including the coil windings, is 2.335 kg.

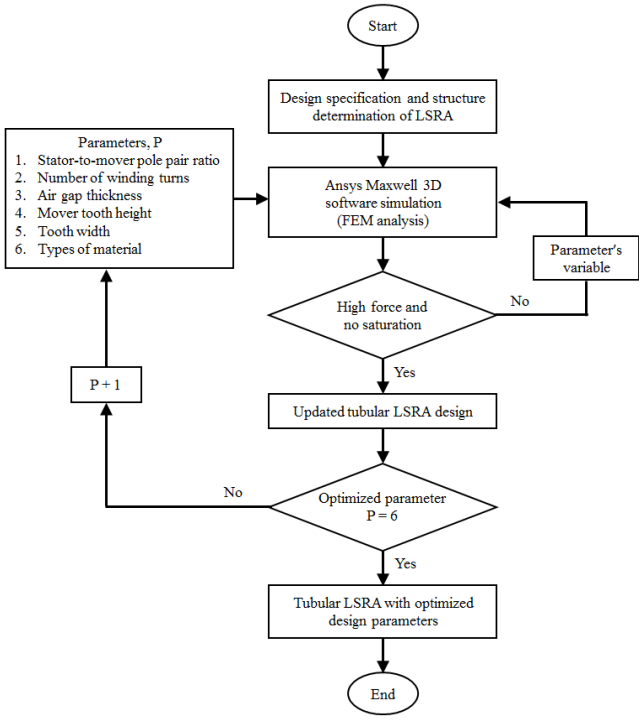

Figure 1 Optimization process sequence

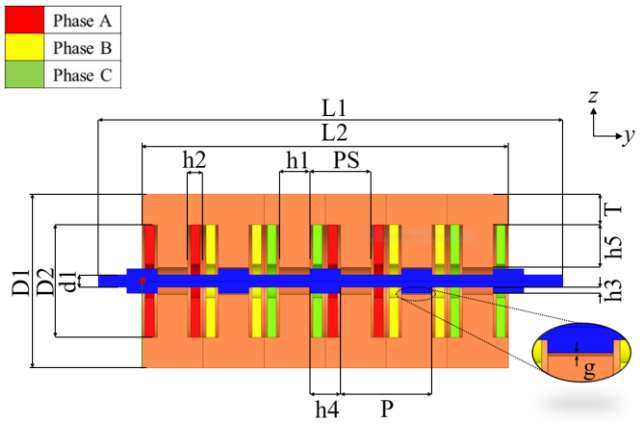

Figure 2 Initial design of tubular LSRA

Table 1 Optimized parameters of tubular LSRA

Parameter	Symbol	Value
Stator to Mover Pole Pairs Ratio	RS:M	12:8
Type of Material	-	S45C
Stator Outer Diameter	D1	57 mm
Stator Inner Diameter	D2	37 mm
Stator Tooth Width	h1	5 mm
Stator Slot Width	h2	2.5 mm
Stator Tooth Pitch	PS	10 mm
Stator Length	L2	120 mm
Stator Tooth Height	h5	14 mm
Stator Yoke Thickness	T	10 mm
Mover Shaft Diameter	d1	5 mm
Mover Tooth Height	h3	1.5 mm
Mover Tooth Width	h4	5 mm
Mover Tooth Pitch	P	15 mm
Mover Length	L1	410 mm
Air Gap Thickness	g	0.5 mm
Winding Turns per Coil	n	60 turns

Figure 4 shows the fabrication procedure for the coil winding. The corkscrew design of the tubular LSRA has a simple disk-shaped hand wounded using enamelled copper wire 0.55 mm in diameter. This disk-shaped coil enables the coil winding to be assembled on both sides of the stator slot. There are 24 coils in total, and each coil has 60 turns. The coil winding was wounded (60 turns per coil) on a mould with thermal sheet insulation paper to achieve the disk-shaped coil. The copper coil winding was sandwiched between the thermal sheet insulation paper (Nomex paper type 410) with 0.1 mm thickness. Then, a thin acrylic resin layer was injected into the coil to maintain its shape once it was removed from the mould. Lastly, the mould was disassembled after the acrylic resin had cured, and the coil winding with two connecting wires protruding was manufactured. The manufactured coil winding's outer diameter (O.D) and inner diameter (I.D) is 37 mm and 10 mm, with a maximum coil winding thickness of 2.4 mm.

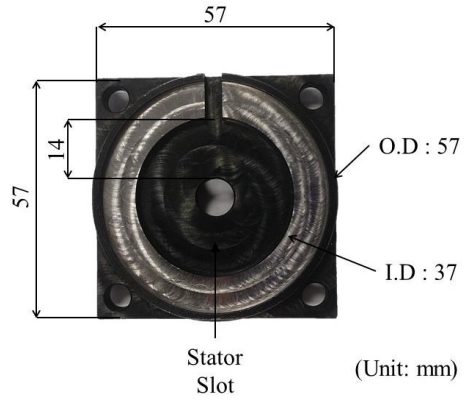

(a) Individually fabricated stator

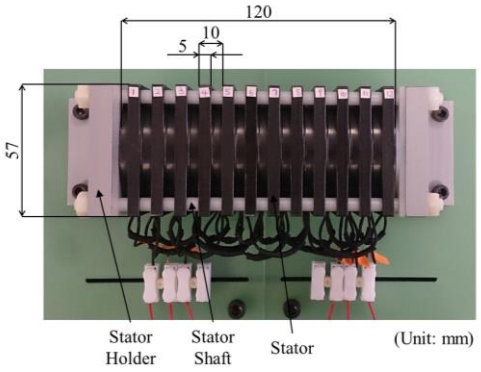

(b) Final stator assembly

Figure 3 Fabricated stator of tubular LSRA prototype

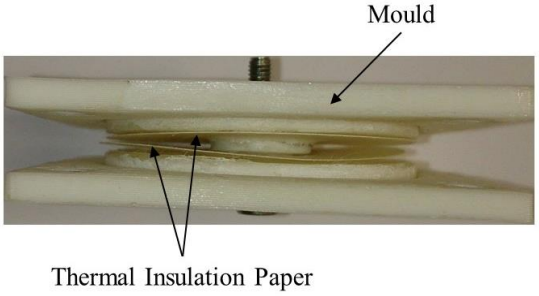

(a) 3D Printed mould with thermal insulation paper

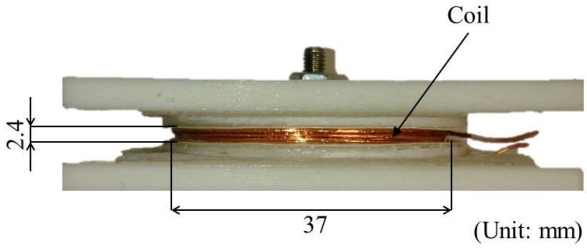

(b) Coil forming with acrylic resin

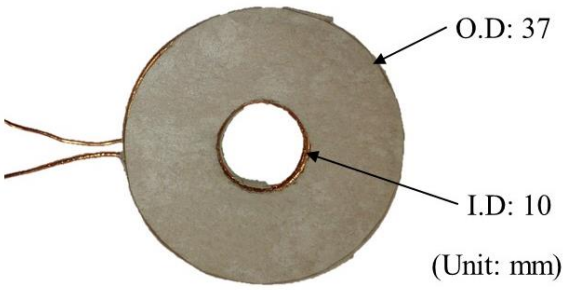

(c) Fabricated disk-shaped stator winding

Figure 4 Fabrication procedure of coil winding

Based on the measured dimension of the stator and copper wire, the stator slot area and the coil winding area can be calculated as shown in Equation 6 to Equation 9.

$$A_{slot} = 2h_2h_5 = 2(2.5)(14) = 70\ mm^2 \quad (6)$$

$$A_{Cu} = \frac{2\pi nd^2}{4} = \frac{2\pi(60)(0.55)^2}{4} = 28.5\ mm^2 \quad (7)$$

$$A_{ins} = 4l_{ins}h_{ins} = 4(0.1)(14) = 5.6\ mm^2 \quad (8)$$

$$A_{coil} = A_{Cu} + A_{ins} = 28.5 + 5.6 = 34.1\ mm^2 \quad (9)$$

where A_{slot} is area of stator slot, h_2 is stator slot width, h_5 is stator tooth height, A_{coil} is area of coil winding, A_{Cu} is area of copper wire, n is number of winding turns, d is diameter of enamelled copper wire, A_{ins} is area of insulation, l_{ins} is insulation width and h_{ins} is insulation height. Therefore, the fill factor can be calculated as shown in Equation 10.

$$F_f = \frac{A_{coil}}{A_{slot}} = \frac{34.1}{70} = 0.487 \quad (10)$$

where F_f is the fill factor.

Based on Equation 10, the calculated fill factor is 0.487, which is in the normal range of fill factors between 0.2 to 0.7 [21, 22]. In this tubular LSRA design, the coil windings in the stator consist of several coils connected in series and distributed in several stator slots with no mover winding. There were eight coil windings per phase connected in series and had a winding resistance of 3.9 Ω for each phase. Figure 5 shows the series connection of a single-phase coil winding with a similar configuration and arrangement used in the FEM analysis, as shown in Figure 6.

Figure 5: Single phase coil winding connection

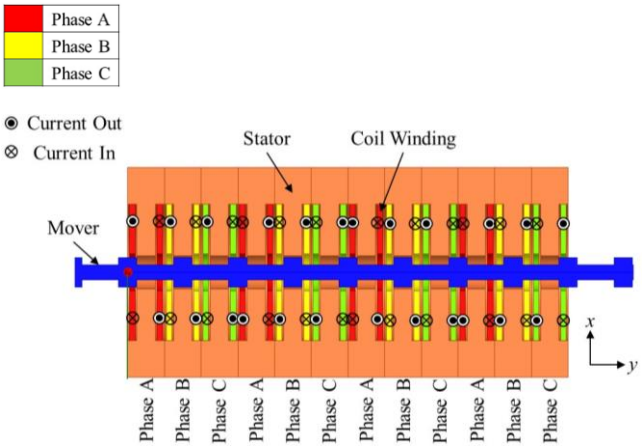

Figure 6 Winding turns configuration

Meanwhile, the actuator's mover is the most crucial part of fabricating the tubular LSRA prototype. The mover is a long shaft with a 5 mm diameter and 1.5 mm mover tooth height, as shown in Figure 7. However, the mover is impossible to be fabricated as the machining process would cause deformation and bending on the mover due to its thin diameter. Therefore, a new mover concept with the same mover dimension was proposed to solve the fabrication constraint. To avoid the bending problem, the mover for the tubular LSRA is separated into three parts, i.e., the mover shaft, the magnetic ring, and the non-magnetic ring. Each mover part was machined separately and precisely. The outer and inner diameters for magnetic and non-magnetic rings are 8 mm and 5 mm to provide 1.5 mm of mover tooth height. The width for both magnetic and non-magnetic rings are 5 mm and 10 mm, respectively.

Meanwhile, the fabricated mover shaft has a diameter of 5 mm with a shaft length of 410 mm. The material used to fabricate both the mover shaft and the magnetic ring is medium carbon steel, S45C, similar to the stator's material. In contrast, the non-magnetic ring is made from MC nylon 901. There are 12 magnetic rings and 11 non-magnetic rings fabricated to provide a traveling distance of 50 mm. Since the mover parts were fabricated separately, the traveling

distance of the actuator can be changed by adding or removing the magnetic rings and non-magnetic rings. Figure 8 shows the fabricated magnetic ring and non-magnetic ring. The non-magnetic rings are used between the magnetic rings as a spacer to ensure the mover tooth pitch is uniform along with the mover. The retaining rings were installed at both ends of the magnetic ring to fix the position of the magnetic ring and non-magnetic ring on the mover shaft. Figure 9 shows the final mover assembly of the fabricated mover. A linear encoder is attached to the linear guide and connected with the mover with a mover block. The mover's weight, including the linear encoder and guide block, is 194.35 g.

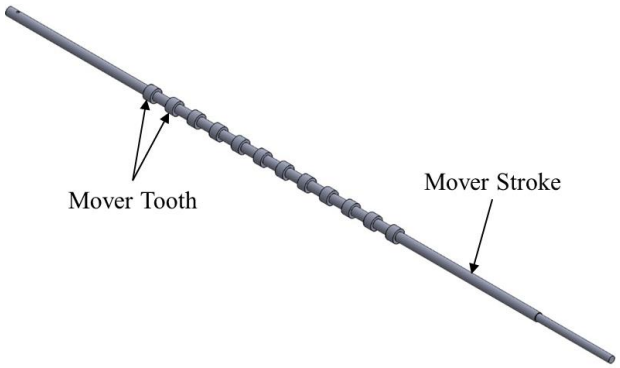

Figure 7 Initial mover design

(a) Magnetic ring (b) Non-magnetic ring

Figure 8 Fabricated magnetic and non-magnetic ring

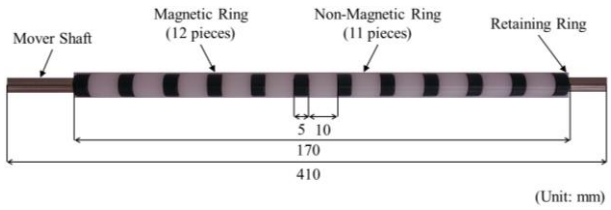

Figure 9 Final mover assembly

In order to operate the tubular LSRA, a proper switching condition is required. The tubular LSRA is operated in a phase-to-phase switching condition based on the mover position. In this research, it is to be noted that forward motion is referred to as the mover moving in the left direction, and reverse motion is referred to as the mover moving in the right direction. Similarly, the forward motion is considered a positive direction and vice versa. By applying the energization sequence AA'-BB'-CC', the mover continuously moves in the forward direction as shown in Table 2. The magnetic circuit for Phase A at the initial mover position is depicted in Figure 10. When the coils on Phase A are applied with excitation current, magnetic flux flows from the stator poles with active phase coils to the mover poles and flows back to the stator poles to form a complete cycle of the magnetic circuit. To reduce the reluctance between the stator and mover poles, the mover poles near the stator poles with active phase coils tend to move toward the stator poles on the left to reach the fully aligned position. When the mover poles moved to the aligned position with stator poles, the active phase coils switched to the next phase. Therefore, the mover will drive in forward and reverse directions continuously according to the active phase coils and mover position sequence. On the other hand, the energization sequence BB'-AA'-CC' makes the mover moves in the reverse direction continuously as shown in Table 3. The complete forward and reverse motion sequences in the first pitch for the tubular LSRA are shown in Table 2 and Table 3. The next following sequence for the next pitch is the repeating of the first pitch. Therefore, only the sequence for the first pitch is shown.

Table 2 Forward motion sequence in the first pitch

Position (mm)	Phase	Stator	Mover
0 – 5	AA'	S1-S4-S7-S10	M3-M5-M7-M9
5 – 10	BB'	S2-S5-S8-S11	M4-M6-M8-M10
10 – 15	CC'	S3-S6-S9-S12	M5-M7-M9-M11

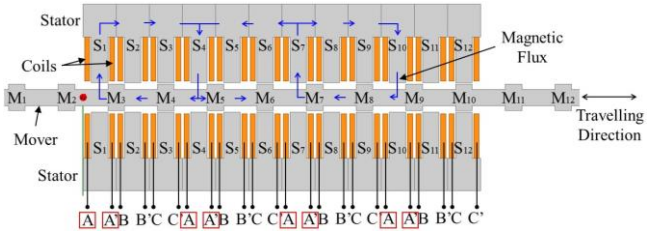

Figure 10 Magnetic circuit for Phase A at the initial position

Table 3 Reverse motion sequence in the first pitch

Position (mm)	Phase	Stator	Mover
0 – 5	BB'	S2-S5-S8-S11	M3-M5-M7-M9
5 – 10	AA'	S1-S4-S7-S10	M2-M4-M6-M8
10 – 15	CC'	S3-S6-S9-S12	M3-M5-M7-M9

3.0 RESULTS AND DISCUSSION

Experimental Setup Overview

Figure 11 shows the overview of the experimental setup. The experiment setup consists of a host computer, digital signal processor (DSP) system (Micro-box), three high current amplifiers (one PBZ60-6.7 by Kikusui Electronic Corporation and two TS250-0 by Accel Instruments), a linear incremental encoder (RGH24W30D33A by Renishaw) and load cell (LRM200

by Futek). The linear encoder and load cell resolutions are 0.2 µm and 0.7 mN, respectively.

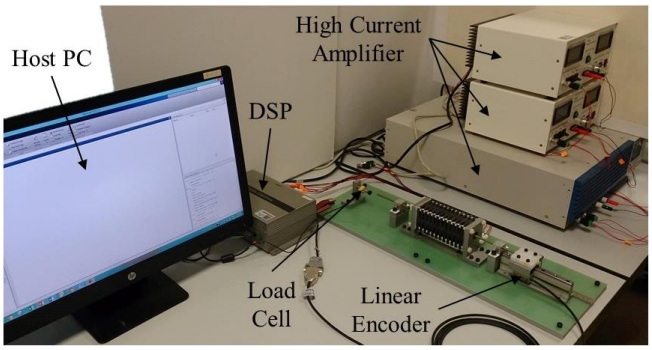

Figure 11 Overall view of the experimental setup

Figure 12 shows the detailed experiment setup of the tubular LSRA prototype. The stators are fixed to the main base by using the stator holders. The main base is made of aluminium, and a thin layer of epoxy glass is placed on the aluminium base for insulation purposes. Two polytetrafluoroethylenes (PTFE) coated linear bushings are accurately aligned and fitted on both the mover's ends in the direction of motion. This is important to ensure the air gap is uniform throughout the actuator and allows low friction sliding surface. A linear encoder read head is mounted on the mover of tubular LSRA and used as a position feedback sensor to measure the displacement of the mover. The load cell measures the thrust force by connecting the load cell and mover with a thin nylon string. The DSP system received the information on the mover's displacement and measured thrust force; meanwhile, it assigned the respective switching signal to three different high current amplifiers to actuate the tubular LSRA.

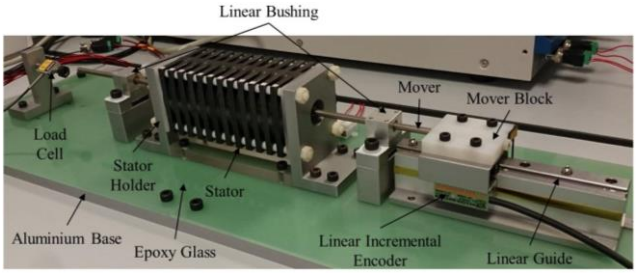

(a) Full view

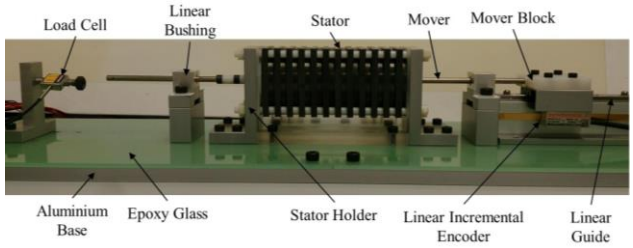

(b) Side view

Figure 12 Final tubular LSRA assembly

Force Characterization

In order to measure the static force characteristic, the mover is fixed at a position by collecting the static force for different rated phase currents. This research, take note that the simulated force is the simulated force obtained from the FEM analysis, whilst the measured static force is the experimental force. The measured static force for each phase was measured at a step of 0.5 mm, and the applied DC excitation current ranges from 1 A to 2 A with 0.5 A increments. The experimental result of static force characteristics concerning mover position and excitation current for a single mover pitch is demonstrated in Figure 13. All three phases demonstrate similar trends in static force generated by the tubular LSRA. As shown in Figure 13, the maximum static force measured by the load cell is 0.24 N and 0.65 N at the rated phase current of 1.5 A and 2.0 A, respectively, at position 6.5 mm. The highest measured static force for each phase and excitation current occurred when the mover position is at the intermediate positions, 2 mm for Phase A, 6.5 mm for Phase B, and 11.5 mm for Phase C. The measured static force started to decrease as the mover moved towards the aligned position and reached the minimum force value when the mover reached the position at 4.5 mm, 9.5 mm, and 14.5 mm for each phase before reaching the fully aligned position. The active phase coils at the stator poles are disconnected at the fully aligned position, and the phase coils for the next stator poles are excited. It is to be noted that the tubular LSRA does not generate any thrust force or motion when the applied excitation current is 1.1 A and below. This is because the thrust force generated by the tubular LSRA is too small, where the generated thrust force could not overcome the maximum static friction force and mass of the mover. Moreover, the tubular LSRA requires at least 1.1 A and above to produce thrust force and motion which will be discussed in Section 5.0.

Figure 14 compares static force characteristics between the generated force and measured force at the maximum rated phase current of 2 A. According to the static force profile, the force generated by the tubular LSRA is within the required range for the semiconductor fabrication application which is between 0.2 N to 1.0 N. Based on the result, the highest and generated static force obtained from the FEM analysis is 0.95 N. Meanwhile, the maximum measured static force obtained from the experimental works is 0.65 N which is reduced by 44.9 % compared to the simulation result. The main reason that causes the reduction in the measured static force is the presence of friction force between the mover shaft and linear bushings. Figure 15 illustrated the measured friction force when the mover was manually pulled. Based on Figure 15, the static and kinetic friction data obtained are relatively close. Therefore, the static and kinetic friction is assumed to be similar, and the average friction force is approximately 0.26 N.

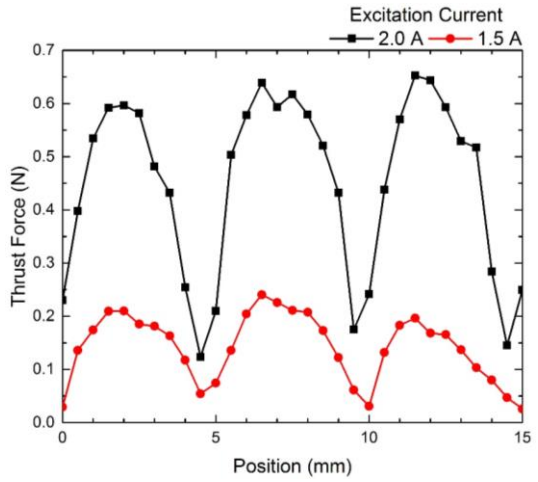

Figure 13 Measured static force characteristics

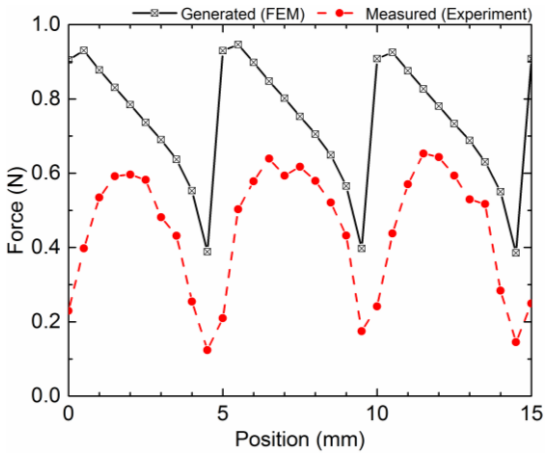

Figure 14 Comparison of generated and measured static force characteristics at 2.0 A

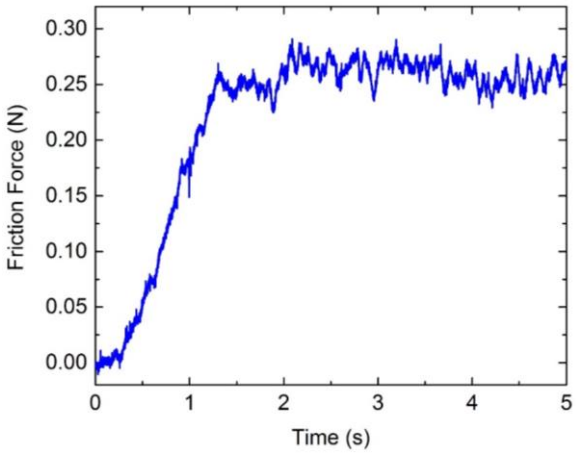

Figure 15 Measured friction force

Besides that, both generated and measured static force acquired similar trends when the mover is moved from an intermediate position (2.5 mm) to an aligned position (4.5 mm) for all three phases, as shown in Figure 14. However, the measured force clearly shows different characteristics than the generated force when the mover moves from an unaligned (0 mm) to the intermediate position (2.5 mm). Unlike the generated static force, which has the highest thrust force at the unaligned position (0 mm), it decreases when the mover moves to the intermediate position (2.5 mm). The measured static force shows an opposite trend. The tubular LSRA has a smaller static force at the unaligned position (0 mm). The static force increases when the mover moves from the unaligned position to the intermediate position. In addition, experimental work shows that the tubular LSRA can generate the most significant thrust force when the mover is at an intermediate position instead of an unaligned position, as shown in the FEM analysis. The difference between the generated and measured static force characteristics is due to the uncontrolled magnetic flux distribution in the tubular LSRA usually occurs in any conventional LSRA design.

Figure 16 shows the magnetic flux distribution when the mover is located at an unaligned position, intermediate position, and nearly aligned position under the maximum rated phase current of 2 A. Both the generated and measured static force profiles were conducted with an interval of 0.5 mm. The fully aligned position is supposed to be 5 mm. However, according to the switching algorithm, the active phase will be switched to the next phase when the mover reaches the aligned position of 5 mm. Besides that, a fabrication tolerance of 20 µm also caused the mover not to reach the exact aligned position at 5 mm. Therefore, the nearly aligned position with 4.5 mm is used in the context of static force profile only because it is the nearest to the aligned position. This is to observe the trends and changes of magnetic flux flow as the mover moves from an unaligned position toward the aligned position. However, the actual fully aligned position during the operation of the tubular LSRA remained at 5 mm.

Based on the results, the magnetic flux distribution on the active stator and mover poles at Phase A was increasingly high when the mover poles moved towards the aligned position. When Phase A is applied with excitation current and the mover is at the unaligned position, the magnetic flux flows from the active stator pole to the mover pole to form a complete magnetic circuit. However, some amount of magnetic flux flows through the non-active pole, resulting in the non-active pole generating a small amount of force that opposes the measured static force. The uncontrolled magnetic flux distribution generally causes the force generated from the non-active pole. While the mover moves from an unaligned position to an intermediate or aligned position, the magnetic flux that flows through the non-active poles is reduced as most of the magnetic flux flows through the active pole due to the increasing overlapping area. The uncontrolled magnetic flux distribution in the tubular LSRA justified the difference in measured static force characteristic when the mover is

at the unaligned position compared to the generated static force characteristic.

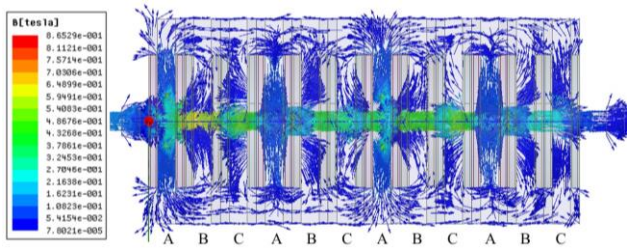

(a) Unaligned position (0 mm)

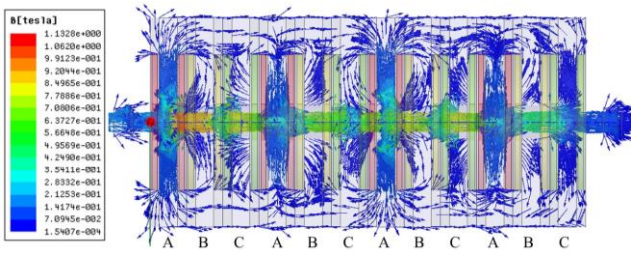

(c) Intermediate position (2.5 mm)

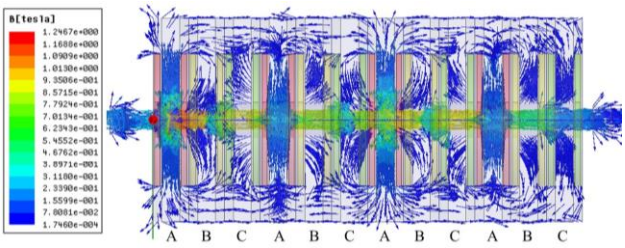

(d) Nearly aligned position (4.5 mm)

Figure 16 Magnetic flux distribution at different mover position

Motion Characterization

In this research, the motion of the tubular LSRA is further examined through driving characteristics via an open-loop experiment. The mover's open-loop motion characteristic is evaluated by applying a constant DC current from 0.9 A to 2 A with 0.1 A increments for four seconds. The excitation phase depends on the mover position, as illustrated in Table 2 and Table 3. The steady-state displacement is collected to observe the motion behaviour of the tubular LSRA. Thus, the relationship between the motion characteristics for forward and reverse motion concerning excitation current can be obtained. Then, the response of the tubular LSRA for a single step motion is evaluated by applying a constant excitation current of 2A for 1s. The transient responses such as percentage of overshoot, settling time, and equilibrium position are collected to determine the behaviour of the tubular LSRA. Next, an open-loop control with continuous step motion is examined to observe the motion characteristic. Six steps (two pitches), forward and reverse motion, are evaluated by applying a constant phase excitation current of 2A in sequence for 1s each step. The displacement of the mover is collected to determine the continuous step motion behaviour of the tubular LSRA in open-loop control. Figure 17 shows the block diagram of the open-loop control for the tubular LSRA, and the respective phase excitation current is illustrated in Figure 18. In Figure 17, the Matlab Simulink block diagram uses the saturation unit block to ensure that the maximum current to the experimental setup does not exceed 2A. This block prevents the winding coils for Phase A, B & C from breakdown. The open-loop control performance is evaluated based on the displacement response.

Another technique to characterize the tubular LSRA is to obtain the mover dynamic responses in terms of displacement, velocity, and acceleration with open-loop control. The mover response is obtained by reciprocating the mover between 0 mm and 25 mm at a maximum rated phase current of 2 A. The experiment was implemented using a switching mechanism based on mover position, as shown in Tables 2 and 3. Therefore, a linear encoder measures the mover position and feeds to the switching mechanism to determine the phase excitation. The switching algorithm will recalculate the mover position when the mover moves exceed 15 mm to determine the phase excitation after the first pitch. This is to simplify the switching mechanism for the repeating sequence. Figure 19 illustrates the block diagram of the switching mechanism for reciprocating motion, i.e., forward and reverse motion, as shown in Figure 20. The switching mechanism was changed to forward motion when the mover reached 0 mm; meanwhile, the reverse motion was applied when the mover reached 25 mm and went back to the initial position (0 mm). Although the maximum traveling distance of the tubular LSRA is 50 mm, the maximum reciprocating range is fixed at 25 mm to prevent the mover from colliding with the linear bushing during open-loop control. In order to acquire the velocity response of the tubular LSRA, the displacement is undergoing the first derivative with respect to time. On the other hand, the acceleration response is obtained when the displacement is undergoing the second derivative with respect to time. The velocity and acceleration responses go through a second-order low-pass filter with a cut-off frequency of 160 Hz to attenuate the high-frequency signals. The mover response obtained holds a piece of important information on the characteristics of the tubular LSRA system.

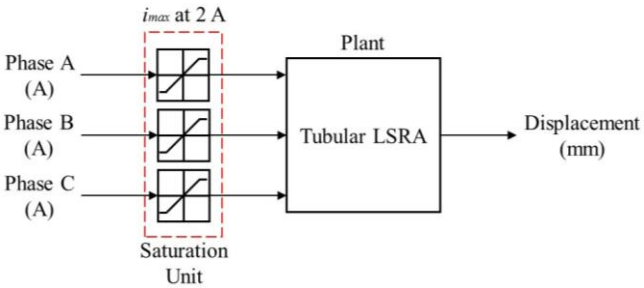

Figure 17 Three-phase open-loop control of tubular LSRA

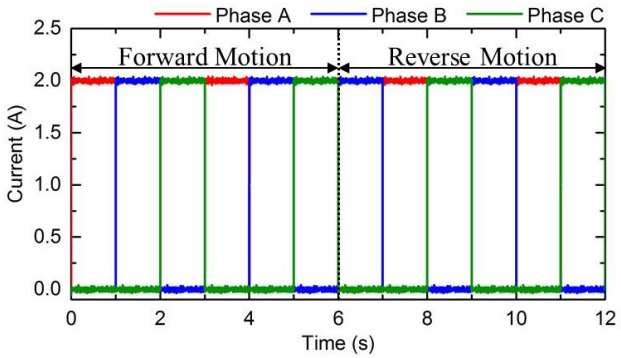

Figure 18: Phase current for three-phase open-loop control

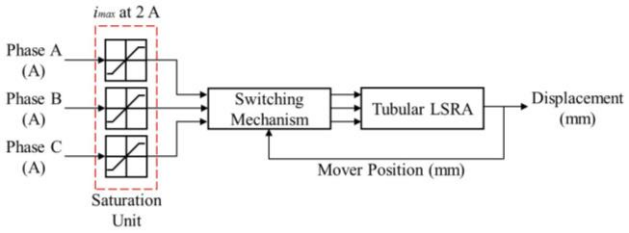

Figure 19 Block diagram of the switching mechanism for the reciprocating motion

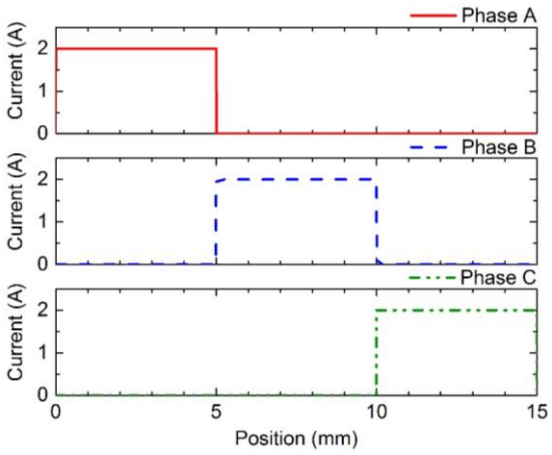

(a) Forward motion

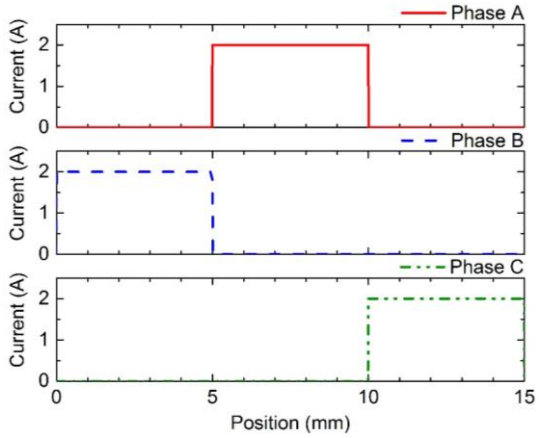

(b) Reverse motion

Figure 20 Switching mechanism

The linear motion characteristic of the tubular LSRA was evaluated experimentally with a series of open-loop experiment control. It is to be noted that forward motion is referred to as the mover moving to the left direction, and reverse motion is referred to as the mover moving to the right direction. Similarly, the forward motion is considered a positive direction and vice versa. The mover displacement of the tubular LSRA with respect to the excitation current for forward motion and reverse motion are presented in Figure 21 and Figure 22. All the three phases for both forward and reverse motion demonstrated similar trends in motion characteristics, in which displacement increased with the increased applied excitation current. By comparison, all the three phases for both forward and reverse motion have their motion characteristics as the displacement versus excitation current curve is different, although their trends are similar. This is because the mover has an unbalanced load on one end of the mover, which causes the tubular LSRA requires more considerable energy to pull the mover. Figure 23 shows the mover structure where the forward part is heavier than the reverse part due to installing the linear encoder and linear guide on the forward part. Besides that, the uncontrolled magnetic flux distribution also causes Phase B, which is located in between Phase A and Phase C, to have higher measured static force and magnetic flux density compared to the Phase A and Phase C. When the applied excitation current is less than 1.1 A, the tubular LSRA is motionless for both forward motion and reverse motion due to the generated thrust force is smaller than the maximum static friction force which already been justified.

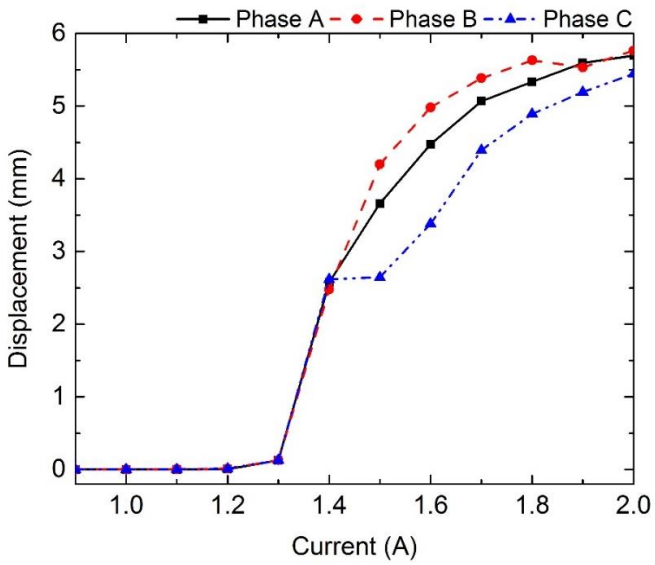

Figure 21 Linear motion characteristic for forward motion

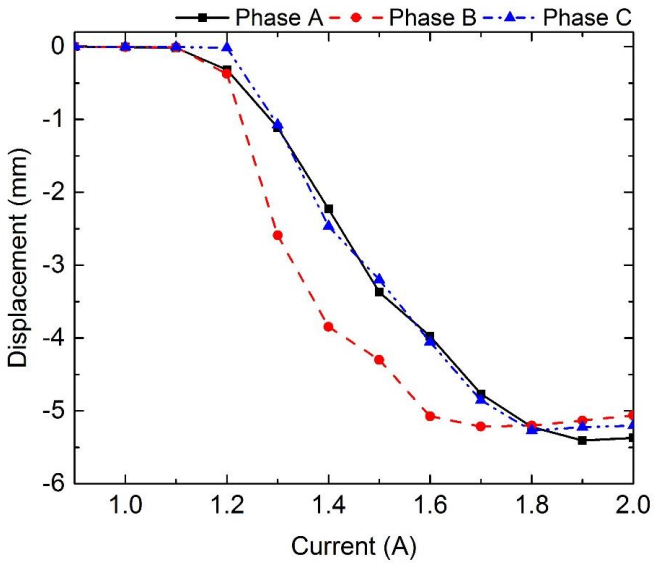

Figure 22 Linear motion characteristic for reverse motion

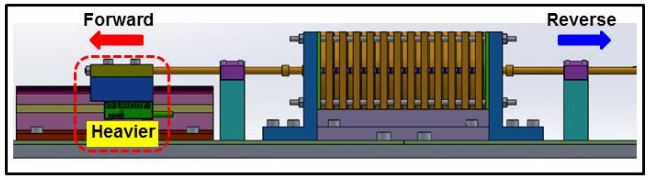

Figure 23 Unbalanced mover load structure

Based on the forward motion characteristic, as shown in Figure 21, the displacement gradually increases when the applied excitation current increases from 1 A to 1.3 A. The mover displacement increases rapidly when the excitation current is increased from 1.3 A to 1.8 A. On the other hand, the reverse motion characteristic in Figure 22 shows that the displacement increased slowly when the applied current was increased from 1 A to 1.2 A. When the excitation current is increased from 1.2 A to 1.8 A, the generated force increases, causing the displacement to increase rapidly, similar as in forward motion. However, the displacement increments for both forward and reverse motions reduced when the applied excitation current was above 1.9 A. When the applied excitation current is 1.9 A and above, the tubular LSRA has a more significant generated thrust force and magnetic co-energy; thus, the mover can reach the equilibrium position closer to the expected position. The generated force is the lowest as the mover reaches the equilibrium position due to the sizeable overlapping area between the poles. In open-loop control of tubular LSRA, each phase of tubular LSRA is capable of providing a step motion of 5 mm when the mover moves from an unaligned position to an aligned position. However, the mover was unable to reach the exact fully aligned position when the mover reached the equilibrium position because the thrust force generated by the tubular LSRA was too low to move the mover to the fully aligned position.

The open-loop control of the tubular LSRA for one step forward motion at a maximum rated phase current of 2 A is demonstrated in Figure 24. Based on the result, the tubular LSRA has an overshoot of 33.3 % and requires approximately 0.18 s for the mover to reach the equilibrium position at 5.071 mm, where the mover pole and stator pole are almost fully aligned. At this position, the insufficient energy produced at the active stator and mover poles cannot attract the mover to the expected equilibrium position. This is because the large overlapping area between the poles causes a small thrust force to be generated. Therefore, the mover stopped at an equilibrium position instead of a fully aligned position at 5 mm.

Meanwhile, the open-loop control for continuous six steps forward and reverse motion at a maximum rated phase current of 2 A is demonstrated in Figure 25, and Table 4 shows the tabulated results for ten repetitions. Based on the result, it can be observed that the tubular LSRA has a resolution of approximately 5 mm per step. Besides that, it can be depicted that all the step motions for forward motion and reverse motion have similar trends. The mover has an overshoot for forward motion and undershoots for reverse motion due to the mass and inertia of the mover. Then, the active poles pulled the mover back to the aligned position and reached the equilibrium position. However, the mover does not reach the expected equilibrium position. When the mover reaches the equilibrium position, the insufficient energy at the active poles unable to attract the mover to the expected equilibrium position due to large overlapping area between the poles and thus small thrust force generated. The disadvantage of this open-loop control is motion characterized by significant overshoot and error as there is no position feedback in the system to correct the position error. Overshoot occurred for each step motion before the mover reached the equilibrium position caused by the inertia. However, no physical vibration was observed in the experimental work when operating in a continuous step motion. Furthermore, open-loop control of the tubular LSRA only allows the actuator to be operated in step motion, and the intermediate position is unachievable.

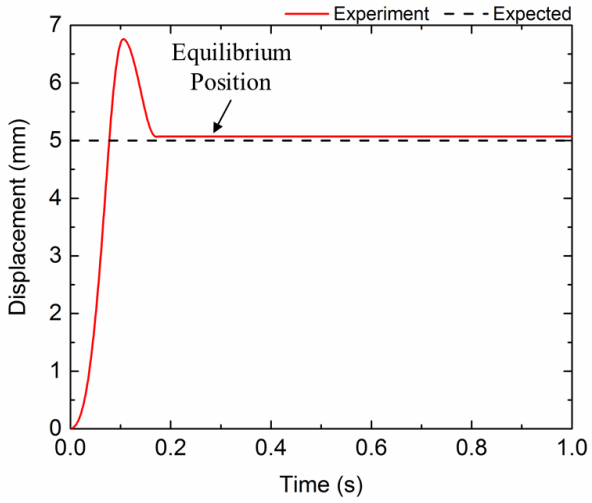

Figure 24 Open-loop control for one step response

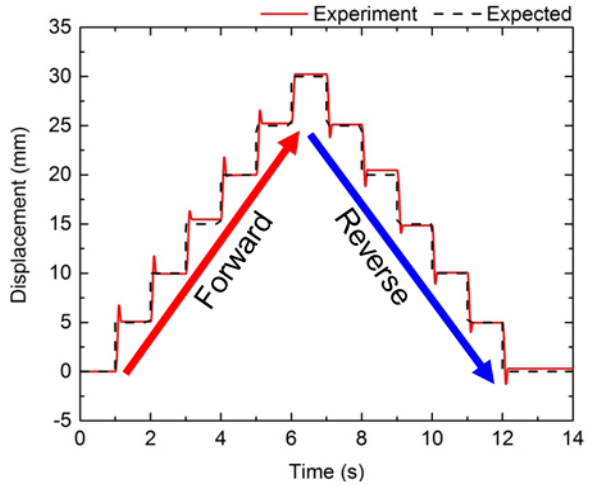

Figure 25 Open-loop control for continuous six steps forward motion and reverse motion

Table 4 Open-loop control for continuous step motion

Motion	Displacement (mm)		Error (mm)	Standard Deviation
	Expected	Average		
Forward	5	5.031	0.031	0.088
	10	9.951	- 0.049	0.067
	15	15.469	0.469	0.040
	20	19.964	- 0.036	0.025
	25	25.230	0.230	0.024
	30	30.208	0.208	0.048
Reverse	25	25.072	0.072	0.049
	20	20.458	0.458	0.035
	15	14.921	- 0.079	0.047
	10	10.079	0.079	0.014
	5	4.971	- 0.029	0.079
	0	0.246	0.246	0.053

Another method to acquire the tubular LSRA performance is to measure the signals of the displacement, velocity, and acceleration responses of the mover while reciprocating at a maximum rated phase current of 2 A. The mover responses based on the open-loop control reciprocating between 0 mm and 25 mm is depicted in Figure 26. It can be seen that the maximum and minimum displacement of the mover exceed the reciprocating range. The linear encoder measured the maximum, and minimum displacements are 28.414 mm and - 3.199 mm instead of 25 mm and 0 mm. This is because the mass of the mover causes inertia when the mover changes direction at 25 mm and 0 mm. Moreover, the open-loop control of the tubular LSRA does not have position feedback and controller; thus, the tubular LSRA cannot correct the position error that occurred in the system.

On the other hand, the maximum velocity at the maximum rated phase current of 2 A is exceeded 200 mm/s. The maximum velocity for forward and reverse motions is 213.64 mm/s and - 196.32 mm/s, respectively. It can be observed that the forward motion has a faster velocity compared to reverse motion due to the mover having more significant inertia in forward motion, which is caused by the unbalanced load on one side of the mover. In addition, it can be observed that the maximum acceleration occurs when the mover is decelerating. When the mover is decelerating, the maximum acceleration is approximately 8 m/s^2. Meanwhile, when the mover moves with increasing velocity, the average acceleration of the mover is approximately 2 m/s^2. The mover's acceleration is lower than deceleration due to the static friction force when the mover is accelerating. The velocity and acceleration responses are in the performance range for the precision mechanism [23]. Moreover, the fluctuation that occurred in the acceleration response cannot be eliminated is caused of the friction force and force ripples when phase switching, which is commonly found in any normal LSRA. However, no physical vibration was observed in the experimental work, although the fluctuation is observed in the acceleration response.

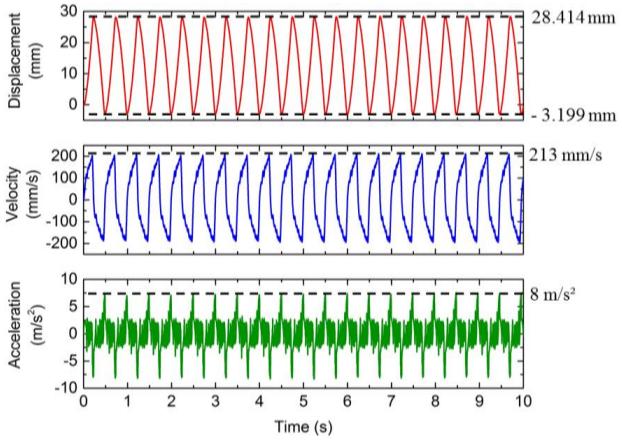

Figure 26 Open-loop control for reciprocating motion

4.0 CONCLUSION

In summary, this research focused on validating the design, optimization, fabrication, and characterization

of the tubular LSRA for application in a low-cost, high-precision system. The velocity and acceleration response of the proposed tubular LSRA met the main performance range for the precision mechanism. The tubular LSRA prototype can produce a maximum measured static force of 0.65 N with a maximum traveling distance of 50 mm. However, the measured static force is approximately 45 % lower than the simulation result, mainly due to the high friction force characteristic and uncontrolled flux distribution in the tubular LSRA system. The maximum velocity and acceleration that the tubular LSRA can operate are approximately 210 mm/s and 8 m/s^2, respectively. However, it can be clearly seen that the fluctuation occurs when the tubular LSRA is accelerating due to the friction force and force ripples when phase switching, which is commonly found in any LSRA and cannot be eliminated but can be reduced by either implementing multi-phase excitation or utilizing power converter. To increase the usefullness of the proposed tubular LSRA, it is essential to include a positioning controller and realize a precision system with the proposed LSRA, which are the plans for future work.

Acknowledgement

This research is funded by the Ministry of Education Malaysia (MOE) under the Fundamental Research Grant Scheme (FRGS) grant no. FRGS/2018/FKE-CERIA/F00353. The authors are grateful to Motion Control Research Laboratory (MCon Lab), Center for Robotics and Industrial Automation (CeRIA), and Universiti Teknikal Malaysia Melaka (UTeM) for supporting the research and publication.

References

[1] Makki, M., and Hemmati, S. 2017. Optimum Design of a Double-sided Permanent Magnet Linear Synchronous Motor to Minimize the Detent Force. *Energy Equipment and Systems*. 5(1): 1-11.

[2] Chowdhury, J., Kumar, G., Kalita, K., Tammi, K., and Kakoty. S.K. 2017. A Review on Linear Switched Reluctance Motor. *Journal of Structural Mechanics.* 50(3): 261-270.

[3] Qiu, H., Hu, K., Yu, W., Yang., C. 2018. Influence of the Magnetic Pole Shape on the Cogging Torque of Permanent Magnet Synchronous Motor. *Australian Journal of Electrical and Electronics Engineering*.14(3-4): 64-70.

[4] Bilgin, O., and Kazan. F. A. 2016. The Effect of Magnet Temperature on Speed, Current and Torque in PMSMs. *22nd International Conference on Electrical Machines (ICEM) 2016.* Lausanne, Switzerland. 2080-2085.

[5] He, H., Zhou, N., Sun. C. 2017. Efficiency Decrease Estimation of a Permanent Magnet Synchronous Machine with Dmagnetization Faults. *Energy Procedia 2017*. 105: 2718-2724.

[6] Hirayama, T., and Kawabata. S. 2017. Study on Design Method for Thrust Ripple Reduction of Double-sided Linear Switched Reluctance Motor. *11th International Symposium on Linear Drives for Industry Applications (LDIA) 2017*. Osaka, Japan. 1-5.

[7] Cheshmeh Beigi, H. M. 2017. Electromagnetic Field Analysis of Novel Low Cogging Force, Linear Switched Reluctance Motor, Based on 2-D Finite Element Method. *Energy Equipment and Systems.* 5(3): 227-240.

[8] Zhang, L., Kou, B., Jin, Y., Chen, Y., and Liu, Y. 2016. Investigation of an Ironless Permanent Magnet Linear Synchronous Motor with Cooling System. *Applied Sciences*. 6(12): 1-12.

[9] Ganji, B., and Askari. M. H. 2016. Analysis and Modeling of Different Topologies for Linear Switched Reluctance Motor using Finite Element Method. *Alexandria Engineering Journal.* 55(3): 2531-2538.

[10] Hirayama, T., Yamashita, S., and Kawabata, S. 2018. Design and Analysis of Linear Switched Reluctance Motor with Coreless HTS Excitation Windings for Ropeless Elevator. *21st International Conference on Electrical Machines and Systems (ICEMS)* 2018. Jeju, Korea. 1879-1884.

[11] Ravikumar, D., Murty, V. S., and Jain., S. 2016. Linear Switched Reluctance Motor for High Speed Transit System. *IEEE Student's Conference on Electrical, Electronics and Computer Science 2016.* Bhopal, India. 1-4.

[12] Luo, X., Zhang, C., Wang, S., Zio, and E., Wang., X. 2018. Modeling and Analysis of Mover Gaps in Tubular Moving-magnet Linear Oscillating Motors. *Chinese Journal of Aeronautics*. 31(5): 927-940.

[13] M. M., Ghazaly, T. A., Yahya, A. C., Amran, Z., Abdullah, M. A. M., Ali, A. H., Jamaludin, N. M., Ali. 2016. Force Characterization of a Tubular Linear Electromagnetic Actuator using Finite Element Analysis Method (FEM). *Jurnal Teknologi.* 78(11): 217-225.

[14] Victor, M. H., Jorge, O., and Fortino. M. 2018. Velocity Regulation in Switched Reluctance Motors Under Magnetic Flux Saturation Conditions. *Mathematical Problems in Engineering*. 1-13.

[15] Kizhakkethil, S. R., and Murugan., S. 2018. Design and Performance Comparison of Permanent Magnet Brushless Motors and Switched Reluctance Motors for Extended Temperature Applications. *Progress in Electromagnetic Research M*. 67: 137-146.

[16] Lenin, N. C., and Arumugam., R. 2015. Design and Experimental Verification of Linear Switched Reluctance Motor with Skewed Poles. *International Journal of Power Electronics and Drive Systems*. 6(1): 18-25.

[17] Hairik, H. A., Thejel, R. H., and Hameed., S. 2015. Speed Control of Switched Reluctance Motor Drive Based on PID Controller. *Basrah Journal for Engineering Sciences.* 15(1): 1-13.

[18] Maslan, M. N., Kokumai, H., and Sato., K. 2017. Development and Precise Positioning Control of a Thin and Compact Linear Switched Reluctance Motor. *Precision Engineering*. 48: 265-278.

[19] Chen, H., Nie, R., and Yan., W. 2017. A Novel Structure Single-Phase Tubular Switched Reluctance Linear Motor. *IEEE Transactions on Magnetics.* 53(11): 1-4.

[20] Li, K., Cheng, G., Sun, X., Yang, Z., Fan, Y. 2019. Performance Optimization Design and Analysis of Bearingless Induction Motor with Different Magnetic Slot Wedges. *Results in Physics.* 12: 349-356.

[21] Okyay, A., Erkorkmaz, and K., Khamesee., M. B. 2018. Mechatronic Design, Actuator Optimization, and Control of a Long Stroke Linear Nano-positioner. *Precision Engineering.* 52: 308-322.

[22] Kumar, P. C., and Geetha., K. 2015. Design, Modeling and Analysis of Linear Switched Reluctance Motor for Ground Transit Applications. *IOSR Journal of Electrical and Electronics Engineering*. 10(1): 1-10.

[23] Oiwa, T., Katsuki, M., Karita, M., Gao, W., Makinouchi, S., Sato, K., and Oohashi., Y. 2011. Questionnaire Survey on Ultra-Precision Positioning. *International Journal of Automation Technology*. 5(6): 766-772.